Practical issues of retrieving isolated attosecond pulses



2009 J. Phys. B: At. Mol. Opt. Phys. 42 134007

(http://iopscience.iop.org/0953-4075/42/13/134007)

J. Phys. B: At. Mol. Opt. Phys. **42** (2009) 134007 (12pp) doi:10.1088/0953-4075/42/13/134007

# Practical issues of retrieving isolated attosecond pulses

**He Wang[1], Michael Chini[1], Sabih D Khan, Shouyuan Chen, Steve Gilbertson, Ximao Feng, Hiroki Mashiko and Zenghu Chang**

J. R. Macdonald Laboratory, Kansas State University, Manhattan, KS 66502, USA

E-mail: chang@phys.ksu.edu

Received 7 April 2009, in final form 7 April 2009
Published 12 June 2009
Online at stacks.iop.org/JPhysB/42/134007

**Abstract**

The attosecond streaking technique is used for the characterization of isolated extreme ultraviolet (XUV) attosecond pulses. This type of measurement suffers from low photoelectron counts in the streaked spectrogram, and is thus susceptible to shot noise. For the retrieval of few- or mono-cycle attosecond pulses, high-intensity streaking laser fields are required, which cause the energy spectrum of above-threshold ionized (ATI) electrons to overlap with that of the streaked photoelectrons. It is found by using the principal component generalized projections algorithm that the XUV attosecond pulse can accurately be retrieved for simulated and experimental spectrograms with a peak value of 50 or more photoelectron counts. Also, the minimum streaking intensity is found to be more than 50 times smaller than that required by the classical streaking camera for retrieval of pulses with a spectral bandwidth supporting 90 as transform-limited pulse durations. Furthermore, spatial variation of the streaking laser intensity, collection angle of streaked electrons and time delay jitter between the XUV pulse and streaking field can degrade the quality of the streaked spectrogram. We find that even when the XUV and streaking laser focal spots are comparable in size, the streaking electrons are collected from a $4\pi$ solid angle, or the delay fluctuates by more than the attosecond pulse duration, the attosecond pulses can still be accurately retrieved. In order to explain the insusceptibility of the streaked spectrogram to these factors, the linearity of the streaked spectrogram with respect to the streaking field is derived under the saddle point approximation.

## 1. Introduction

Single isolated attosecond pulses have recently been demonstrated as indispensable tools for probing fast electron dynamics in gaseous atoms [1–4], in molecules [5] and in condensed-matter systems [6] with unprecedented temporal resolution. For the characterization of such extreme ultraviolet (XUV) pulses, the near-infrared (NIR)-assisted attosecond streaking technique is used, whereby the momentum of photoelectrons ionized by the XUV pulse in the presence of a NIR streaking field is measured as a function of the time delay between the XUV and NIR pulses [7–11]. Such measurement yields a two-dimensional spectrogram of delay and electron energy, in which the intensity and phase of both the XUV pulse and NIR streaking field are encoded. Mairesse and Quéré (2005) proposed the use of the principal component generalized projections algorithm (PCGPA) [12] for reconstruction of the attosecond pulse from the streaked spectrogram, a technique called frequency-resolved optical gating for complete reconstruction of attosecond bursts (FROG-CRAB) [13], which we will refer to only as CRAB. Using this method, a single 130 as XUV pulse generated by polarization gating was successfully retrieved from the streaking spectrogram [9]. Furthermore, 80 as single attosecond XUV pulses generated by amplitude gating were recently retrieved from the streaking spectrogram [10]. However, several practical issues of retrieving attosecond pulses from such two-dimensional spectrograms have hardly been addressed so far. Here we study the effects of five major factors on the pulse retrieval using PCGPA: the count rate, the streaking speed, the streaking laser intensity variation, the collection angle of streaked electrons and the time jitter between the XUV pulse and the streaking field.

[1] These authors contributed equally to this work.

 

## 2. CRAB basics

Once the atoms with ionization potential $I_p$ absorb XUV photons, free electrons with momentum $\mathbf{p}$ are produced through the dipole transition $d(\mathbf{p})$ from the ground state. Then the strong NIR field introduces a momentum shift to those electrons. The kinetic energy, $W = p^2/2$, of the free electron is measured as a function of the delay $\tau$ between the XUV and NIR pulses to construct a spectrogram. In atomic units, the streaked electron spectrogram is expressed as [11, 13, 14]

$$S(W,\tau) = \left| \int_{-\infty}^{\infty} E_{\mathrm{X}}(t) d[\mathbf{p} + \mathbf{A}_{\mathrm{L}}(t+\tau)] \exp[-\mathrm{i}\varphi(\mathbf{p}, t+\tau)] \times \exp[-\mathrm{i}(p^2/2 - \Omega_{\mathrm{X}} + I_{\mathrm{p}})t]\mathrm{d}t \right|^2, \quad (1)$$

$$\varphi(\mathbf{p}, t) = \int_t^{\infty} \left[ \mathbf{p} \cdot \mathbf{A}_{\mathrm{L}}(t') + \frac{1}{2} |\mathbf{A}_{\mathrm{L}}(t')|^2 \right] \mathrm{d}t', \quad (2)$$

where $E_{\mathrm{X}}(t)$ is the complex field amplitude of the XUV pulse to be characterized. For simplicity, here we assume that the XUV pulse has a Gaussian shape as expressed by

$$E_{\mathrm{X}}(t) \propto \exp\left[-2\ln(2)t^2(1+\mathrm{i}\xi)\big/\tau_0^2(1+\xi^2)\right]. \quad (3)$$

Here, $\tau_0$ is the transform-limited XUV pulse duration, $\xi$ is the chirp of the XUV pulse, and the XUV pulse duration $\tau_{\mathrm{X}}$ is related to the chirp as $\tau_{\mathrm{X}} = \tau_0\sqrt{1+\xi^2}$. $\Omega_{\mathrm{X}}$ is the central XUV photon energy. $\mathbf{A}_{\mathrm{L}}(t)$ is the vector potential of the NIR pulse. When the NIR electric field is expressed as $\mathbf{E}_{\mathrm{L}} = \mathbf{E}_0(t)\cos(\omega_{\mathrm{L}}t)$, where $\omega_{\mathrm{L}}$ is the carrier frequency and $\mathbf{E}_0(t)$ is the envelope of the NIR pulse assumed as Gaussian shape, the vector potential becomes $\mathbf{A}_{\mathrm{L}} = -\mathbf{E}_0(t)/\omega_{\mathrm{L}}\sin(\omega_{\mathrm{L}}t)$ under the slowly varying envelope approximation.

In equation (1), the momentum shift of the classical electron can be understood as a phase modulation of the quantum electron wave packet by the laser field. The phase modulation $\varphi(\mathbf{p}, t)$ is expressed in equation (2). To understand the physical mechanisms of the phase modulation, we can assume the dipole transition element $|d(\mathbf{p})|^2$ to be constant, since the energy bandwidth of the ionized electrons is narrow compared to the central energy. Under the central momentum approximation we obtain

$$G(t) = \exp\left\{-\mathrm{i}\int_t^{\infty} [\mathbf{p}_0 \cdot \mathbf{A}_{\mathrm{L}}(t') + \frac{1}{2}\left|\mathbf{A}_{\mathrm{L}}(t')\right|^2]\mathrm{d}t'\right\}, \quad (4)$$

This measured spectrogram matches the form of CRAB and can be used for reconstruction. Mathematically, the new trace is

$$\hat{S}(W,\tau) \approx \left| \int_{-\infty}^{\infty} E_{\mathrm{X}}(t) G(t+\tau) \times \exp[-\mathrm{i}(p^2/2 - \Omega_{\mathrm{X}} + I_{\mathrm{p}})t]\,\mathrm{d}t \right|^2. \quad (5)$$

This expression has the same form as the FROG trace for conventional laser pulse characterization. The phase modulation acts as a temporal phase gate in the FROG language [13].

Since the gate function is a pure phase modulator $G(t) = \mathrm{e}^{-\mathrm{i}\varphi(t)}$, the total phase $\varphi(t)$ can be written as $\varphi(t) = \varphi_1(t) + \varphi_2(t) + \varphi_3(t)$, with

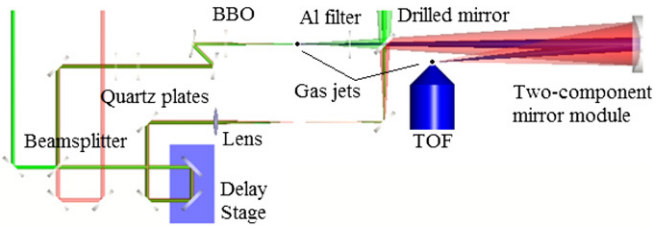


**Figure 1.** Typical setup for the measurement of attosecond pulses consisting of a Mach–Zender configuration. A NIR laser pulse is focused on the first gas jet for attosecond XUV pulse generation. An aluminium filter (Al filter) is used for chirp compensation of the XUV pulse, as well as to block the residual NIR beam. A coated mirror is used to focus the XUV photons to the second gas jet, where the NIR streaking field is superimposed on the XUV focal spot. The momentum spectrum of the streaked electrons falling within the cone of acceptance is measured by a time-of-flight detector (TOF). The green beam is used for locking the interferometer.
(This figure is in colour only in the electronic version)

$$\varphi_1(t) = \int_t^{\infty} \mathrm{d}t\, U_{\mathrm{p}}(t), \quad (6)$$

$$\varphi_2(t) = -\left(\sqrt{8WU_{\mathrm{p}}(t)}/\omega_{\mathrm{L}}\right)\cos\theta\cos\omega_{\mathrm{L}}t, \quad (7)$$

$$\varphi_3(t) = (U_{\mathrm{p}}(t)/2\omega_{\mathrm{L}})\sin(2\omega_{\mathrm{L}}t), \quad (8)$$

where $U_{\mathrm{p}}(t) = E_0^2(t)\big/4\omega_{\mathrm{L}}^2$ is the ponderomotive potential, and $\theta$ is the observation angle relative to the polarization of NIR pulses [13].

Except where otherwise noted, in the simulation and discussion below the NIR pulse was assumed to be 5 fs in duration with a peak intensity of $1 \times 10^{12}$ W cm$^{-2}$ and centred at 800 nm. The XUV spectrum was assumed to support a 90 as transform-limited pulse with a 5000 as$^2$ linear chirp ($\xi \approx \sqrt{3}$) as the intrinsic chirp of the attosecond pulse for the short trajectory electrons, $\theta$ was set at zero to maximize the streaking effect, and the delay range was chosen to be 10.67 fs with a grid size of $512 \times 512$ pixels for the CRAB trace.

## 3. Shot noise

Experimentally obtained CRAB traces, unlike their optical FROG counterparts, are plagued by low count numbers in the spectrogram. A typical setup, such as that shown in figure 1 [15], consists of a laser focused to a gas jet for isolated attosecond pulse generation. The number of XUV photons generated in a noble gas is on the order of $10^6$–$10^7$ per laser shot [16], very small compared to the photon number of femtosecond NIR lasers. After the XUV photons pass through the residual gas in the chamber from the first jet and the Al filter with a thin layer of $Al_2O_3$, the number can be reduced to as little as 10%. Further reductions occur from the low reflectivity of the XUV reflecting optics used in the system as well as small acceptance angles and low quantum efficiency in the detection of the photoelectrons.

The most limiting factor in the count rate is the probability that an XUV photon is absorbed at the second gas jet to generate a photoelectron. The atomic gases used for photoelectron production have photoabsorption cross sections

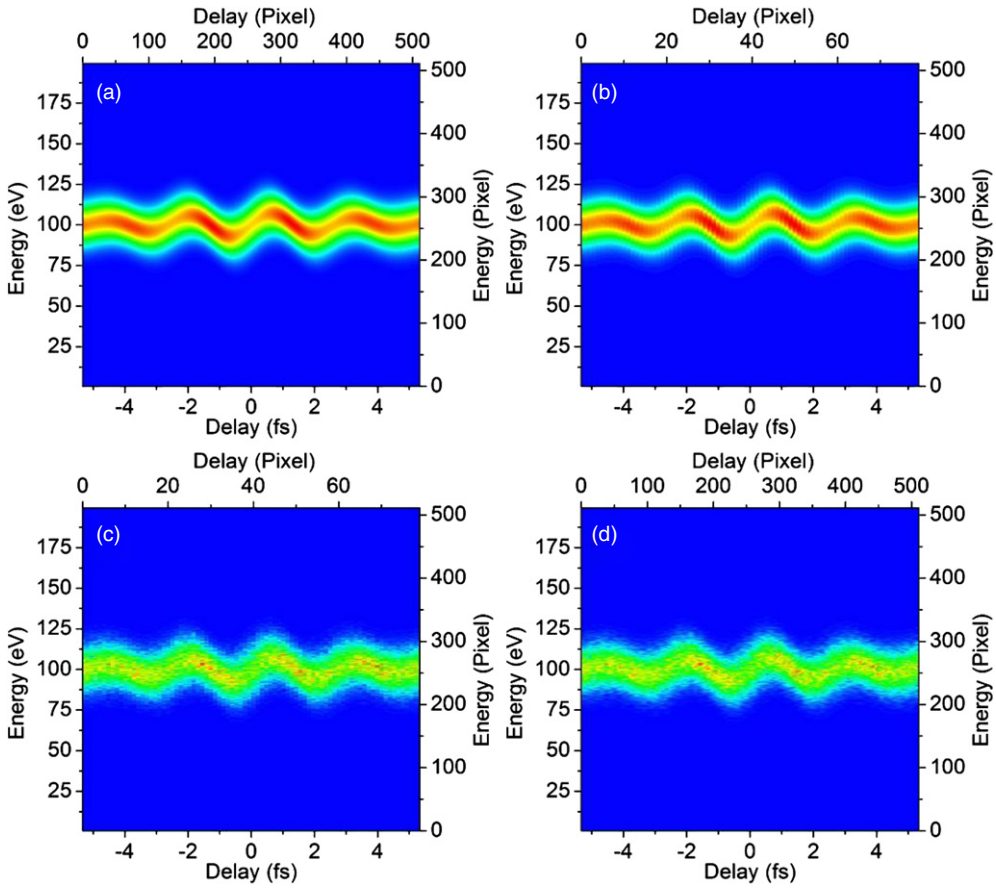


**Figure 2.** Preparation of simulated CRAB traces. All plots are normalized. The XUV spectrum supported a 90 as transform-limited pulse duration and had 5000 as$^2$ linear chirp. The NIR streaking field had a peak intensity of $1 \times 10^{12}$ W cm$^{-2}$. (a) Noise-free trace on a square grid size of $512^2$ pixels. (b) The trace was first resampled to 80 delay steps of ∼130 as with integer values of counts at each pixel. Here, the maximum pixel count was set to 50. (c) After resampling, shot noise was added as integer values taken from a Poisson distribution centred at zero and with variance equal to the number of counts at each particular pixel. (d) The trace was finally interpolated (using a bicubic spline method) back to a square grid of $512^2$ pixels as required for PCGPA.

(This figure is in colour only in the electronic version)

on the order of $10^{-17}$ cm$^2$ at XUV wavelengths [17]. The absorption probability is also a function of the pressure-length product, and the gas pressure is limited by the microchannel plate detector, which requires a vacuum below $10^{-5}$ torr to avoid damage. Even if the local gas density is maximized by using small gas jets and high backing pressures, the gas density is limited by electron scattering and the probability of photoelectron production is less than 1%. Altogether, attosecond streak cameras with typical XUV-coated mirrors, a typical acceptance angle and typical detectors further reduce the overall efficiency of photoelectron detection to $10^{-6}$–$10^{-7}$. The low XUV flux from the source and the poor overall detection efficiency limits the number of detected photoelectrons to ∼1 per laser shot.

For such a small number of photoelectrons, statistical counting error or shot noise can significantly affect the integrity of the streaked spectrogram unless the spectra are recorded for many laser shots. Isolated attosecond pulse generation from all schemes demonstrated so far requires high power, carrier-envelope (CE) phase-stabilized laser pulses [7, 9, 10, 15, 18, 19]. Such pulses with uniform pulse energy [20], duration and CE phase [21] are difficult to maintain over a period of even a few hours, making it a challenge to obtain a sufficiently large statistical sample such that shot noise is negligible. It is thus important to determine how many photoelectron counts are necessary for accurate reconstruction of the attosecond pulse in the presence of shot noise.

### *3.1. Simulation of shot noise in CRAB traces*

To simulate shot noise in the traces, the spectrogram, shown in figure 2(a), was resampled to 80 delay steps with a step size of ∼130 as in order to simulate achievable experimental delay resolution [10, 11, 15]. The energy scale was kept at 512 samples, giving a resolution of ∼0.4 eV, which is similar to the energy resolution of previous experiments [10, 15]. In PCGPA, the delay and energy step sizes, $\delta\tau$ and $\delta E$ respectively, must satisfy the constraint $\delta E \delta\tau = 2\pi/N_{\mathrm{E}}$, where $N_{\mathrm{E}}$, a power of 2, is the total number of samples in energy [11–13]. Experimental CRAB traces must be interpolated in order to satisfy this condition.

The number of counts on each grid point was quantized to integer values with a maximum count of 200, 100, 50, 25 and 10 counts (corresponding to roughly 10000, 5000, 2500, 1250

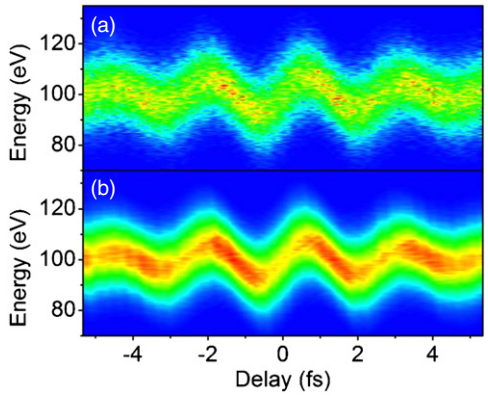


**Figure 3.** (a) Detail of interpolated trace given as input to the PCGPA algorithm, reproduced from figure 2(d). (b) Detail of reconstructed pulse after 1000 iterations of PCGPA. The FROG error was 5.6%. Clearly, the algorithm has retrieved a trace which qualitatively matches the features of the noise-free trace in figure 2(a) more closely than the noisy trace which it was given. (This figure is in colour only in the electronic version)

and 500 total photoelectron counts per delay step), as shown in figure 2(b) for a maximum pixel count of 50. Shot noise, which follows a Poisson distribution with mean value zero and variance equal to the number of counts at a particular pixel, was simulated using a Monte Carlo method and added to the trace, as shown in figure 2(c). Finally, bicubic spline interpolation was performed on the trace to return it to a grid size of 512 × 512 pixels suitable for reconstruction with PCGPA, as shown in figure 2(d). Clearly, the final spectrogram trace with added shot noise in figure 2(d) is quite dissimilar from the noise-free trace in figure 2(a). For a more comprehensive study of the effects of shot noise, this process was performed for pulses with spectrum supporting 90 and 180 as transform-limited pulses for several streaking laser intensities and linear chirps.

### 3.2. *Effects of shot noise on the CRAB reconstruction*

Figure 3 shows the CRAB reconstruction after 1000 iterations for a spectrogram trace with a maximum pixel count of 50 and shot noise added. Qualitatively, the reconstructed trace in figure 3(b) matches more closely to the noise-free trace in figure 2(a) than it does to the trace with shot noise added shown in figure 3(a), which is reproduced from figure 2(d).

In order to quantitatively determine the convergence of a FROG algorithm, the FROG error is typically used. The FROG error indicates the degree to which the retrieved and experimental FROG traces match. However, a trace with noise added is fundamentally an incorrect trace and is likely unphysical. It is thus more useful to define a convergence criterion that indicates how well the algorithm has converged to both the noisy trace and the noise-free trace.

We utilize the convergence criterion described by Fittinghoff for optical FROG traces [22], and consider convergence to have occurred in a trace with added noise for

$$R = \varepsilon\left[\tilde{I}^{\mathrm{FROG}}, I^{\mathrm{FROG}}\right] / \varepsilon\left[I_{\mathrm{n}}^{\mathrm{FROG}}, I^{\mathrm{FROG}}\right] < 2, \qquad (9)$$

where

$$\varepsilon[A, B] = \left[\frac{1}{N^2}\sum_{i=1}^{N}\sum_{j=1}^{N}(A_{ij} - B_{ij})^2\right]^{1/2} \times \left[\frac{1}{N^2}\sum_{i=1}^{N}\sum_{j=1}^{N}B_{ij}^2\right]^{-1/2}, \qquad (10)$$

$I^{\mathrm{FROG}}$ is the noise-free trace, $I_{\mathrm{n}}^{\mathrm{FROG}}$ is the trace with noise added, and $\tilde{I}^{\mathrm{FROG}}$ is the reconstructed trace. In equation (10), $A_{ij}$ and $B_{ij}$ represent the pixel located at coordinate $(i, j)$ in each two-dimensional trace and $N$ is the number of pixels in each dimension. In our case, $I_{\mathrm{n}}^{\mathrm{FROG}}$ was interpolated to a grid of 512 × 512 pixels before calculating the convergence criterion. The critical criterion for convergence is set to $R$ less than 2 rather than 1 because the algorithm is given only the noisy trace as input, and we thus cannot expect it to reproduce the noise-free trace.

In fact, as is shown in figure 4, $R$ is found to be much less than 1 for all values of the maximum pixel count regardless of the XUV bandwidth and NIR streaking intensity ($5 \times 10^{11}$–$2 \times 10^{12}$ W cm$^{-2}$), indicating that the algorithm converges to a solution much closer to the noise-free CRAB trace than to the noisy trace which it was given. This is similar to the case of optical FROG in the presence of noise [22], and is likely due to the significant redundancy contained in the CRAB trace. In fact, the attosecond pulse itself contains only $2N_\tau$ degrees of freedom, where $N_\tau$ is the number of delay steps after interpolation, whereas the CRAB trace has $N_\tau N_{\mathrm{E}}$ degrees of freedom. Also, the attosecond pulse is completely encoded in a single cycle of the CRAB trace, whereas the results shown here are for 4-cycle traces. Because of this significant redundancy, the algorithm is able to effectively ignore the noise and retrieve something more closely related to the noise-free trace. Moreover, the noisy trace is unlikely to correspond to a physical result [12, 22], as the noise generally does not satisfy the intensity constraint of PCGPA. In fact, the vast majority of two-dimensional maps do not correspond to CRAB traces of physical pulse and gate combinations. The algorithm, however, can retrieve only a physically allowed trace corresponding to a unique XUV pulse and streaking field combination.

### 3.3. *The effects of shot noise on XUV pulse retrieval*

The retrieved attosecond XUV pulse intensity and phase are shown for the cases of 200 and 10 counts in figure 5(a). Also, as is shown in (b), the noise in the wings of the pulse is much larger for fewer counts. The full-width at half-maximum (FWHM) pulse duration and the linear chirp for our retrievals are plotted in figure 6. For CRAB traces with at least 50 counts for the maximum pixel, we find that we are able to retrieve the pulse duration and linear chirp within 5% of their actual values when the streaking intensity is greater than $5 \times 10^{11}$ W cm$^{-2}$ for XUV pulses with spectrum supporting 90 as transform-limited durations. These values are similar to the experimental error in previous measurement of sub-100 as pulses [10]. Similarly, when the XUV spectrum supports

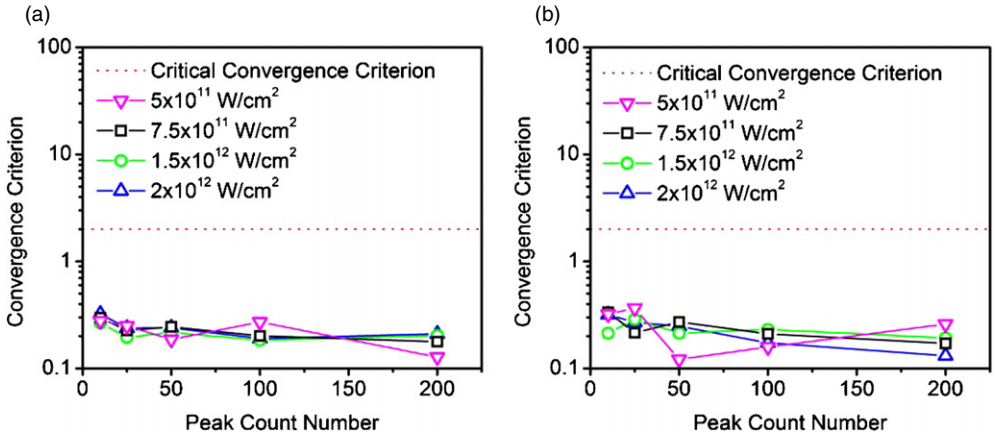


**Figure 4.** Convergence criterion of the retrieved CRAB traces for several streaking intensities from $5 \times 10^{11}$ to $2 \times 10^{12}$ W cm$^{-2}$. (a) XUV spectrum supporting 90 as transform-limited pulses, with 5000 as$^2$ linear chirp. (b) XUV spectrum supporting 180 as transform-limited pulses, with 5000 as$^2$ linear chirp. For all values of peak count number, the convergence criterion is less than 1.
(This figure is in colour only in the electronic version)

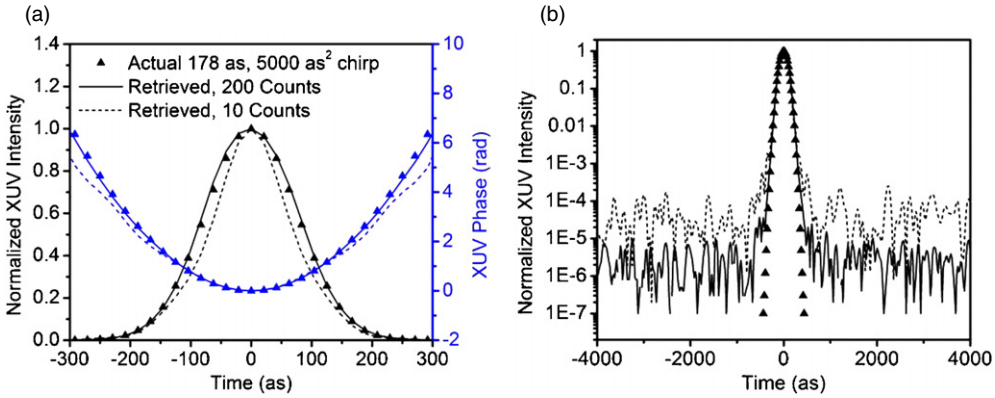


**Figure 5.** (a) Normalized XUV intensity and phase. (b) Normalized XUV intensity on log scale. The streaking intensity was $1 \times 10^{12}$ W cm$^{-2}$. The triangles show the noise-free pulse, whereas the solid line and dashed line show the retrieved pulses with 200 counts and 10 counts at the peak of the energy spectrum, respectively.
(This figure is in colour only in the electronic version)

180 as transform-limited pulses, we are able to retrieve the pulse duration within 3% and the linear chirp within 5% for traces with 50 counts or more. However, as the number of counts is further decreased, the algorithm begins to severely miscalculate the pulse duration, indicating that it has failed to converge to an accurate result. Our simulations indicated that the pulse durations were underestimated for pulses with large values of $\xi$, whereas they were overestimated for nearly transform-limited pulses.

### *3.4. Effects of count rate on experimental data*

In order to further test the pulse retrieval with CRAB, experimental attosecond streaking data was used [15]. The isolated attosecond pulses were generated with the double optical gating [19]. Because our data acquisition system saves the photoelectron energy spectrum recorded for each laser shot, we are easily able to select only a sample of data taken within a given time frame. In the experiment, the photoelectron energy was measured at 32 delay steps with a step size of 333 as for 60 s, or around 55 000 laser shots, each. The spectral bandwidth supported attosecond pulses with transform-limited pulse durations of 137 as. The detector had 100 energy channels spanning 50 eV, and a resolution of 0.7 eV determined by the precision of our timing electronics and the length of the TOF tube. By analysing only the data from selected laser shots, we can observe what the resulting CRAB trace would be for accumulation times less than 60 s.

Figure 7 shows the reconstructed attosecond temporal profile and phase for effective accumulation times of 60 and 2 s (corresponding to total photoelectron counts of roughly 24 500 and 800 for each delay step). It is important to note that the measured CRAB traces are corrected for background noise, such as above-threshold ionization electron counts, and the dipole transition matrix element corresponding to the measured photoelectron momentum before reconstruction. However, such a correction is easily made and is independent of the shot noise. As can be seen in figures 7(a) and (b), a decrease in the accumulation time by more than an order of magnitude yields only small differences in the temporal profile

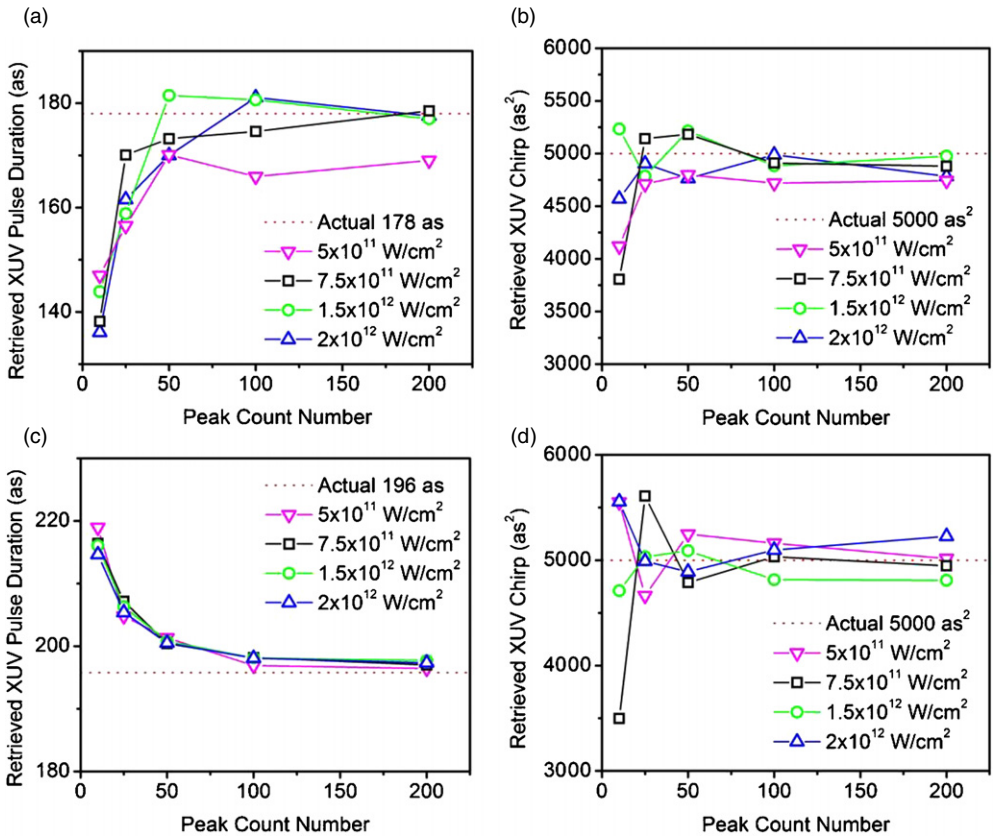


**Figure 6.** (a) Retrieved XUV pulse duration and (b) retrieved linear chirp for pulses with spectrum supporting 90 as transform-limited pulses. For peak count numbers above 50, the pulse duration and linear chirp are retrieved within 5% of their actual values for streaking intensities greater than $5 \times 10^{11}$ W cm$^{-2}$, indicating convergence of the algorithm. (c) Retrieved XUV pulse duration and (d) retrieved linear chirp for pulses with a spectrum supporting 180 as transform-limited pulses. For peak count numbers above 50, the pulse duration is retrieved within 3% and the linear chirp within 5% of their actual values.

(This figure is in colour only in the electronic version)

and phase of the reconstructed XUV pulse. Figure 7(c) shows the same temporal profiles as in (a) on a log scale. A substantial increase in the noise in the wings of the pulse is present, just as in the simulated pulses. Such an error in the wings of the pulse is to be expected, due to the small number of photoelectron counts corresponding to the low-intensity portions of the pulse. Figure 7(d) shows the FWHM pulse duration for the different retrievals, as a function of the peak count number. The peak count number here must include the shot noise, as it is taken from experimental data.

## 4. Streaking speed

Classically, streaking can be understood as the momentum shift of a free electron by the NIR field. According to the Rayleigh criterion, in order to resolve two events separated by $\Delta t$ in time, they must be shifted with respect to each other by at least as much as their own spectral width [2, 8]. When the quiver energy $U_p(t) = E_0^2(t)/4\omega_L^2$ is much less than central energy $W_0 = p_0^2/2$, the minimum XUV pulse duration that can be measured is determined by [2]

$$\delta t = \frac{T_L}{2\pi}\sqrt{\frac{\omega_L}{\Delta W}}, \tag{11}$$

where $T_L$ is the period of the NIR field, and $\Delta W$ is the energy shift caused by the NIR streaking field. Using this criterion for a NIR laser centred at 800 nm, in order to resolve a sub-100 as XUV pulse centred at 60 eV such as was generated most recently [10], at least 28 eV of $\Delta W$ is required, which corresponds to the minimum NIR laser peak intensity of $5.5 \times 10^{13}$ W cm$^{-2}$. Such a high intensity of the NIR field can produce free electrons through multi-photon ionization and above-threshold ionization (ATI). Since the cutoff energy of rescattered electrons from ATI can reach $10U_p(\sim 33$ eV), the ATI electrons overlap with the streaked XUV photoelectrons and add significant background noise to the CRAB trace [14, 23]. To minimize the effect of the ATI background, in the early experiments the streaked electrons were collected perpendicular to the polarization of the NIR and XUV pulses [7, 24].

When the CRAB trace is used to characterize the XUV pulse, the measurement of the attosecond pulse is converted into a 2D phase retrieval problem, which is well known in many other fields [25]. In principle, since the 2D trace has redundant information and phase retrieval in two or more dimensions essentially always yields a unique solution [25], the high streaking speed required by the Rayleigh criterion above may not be necessary.

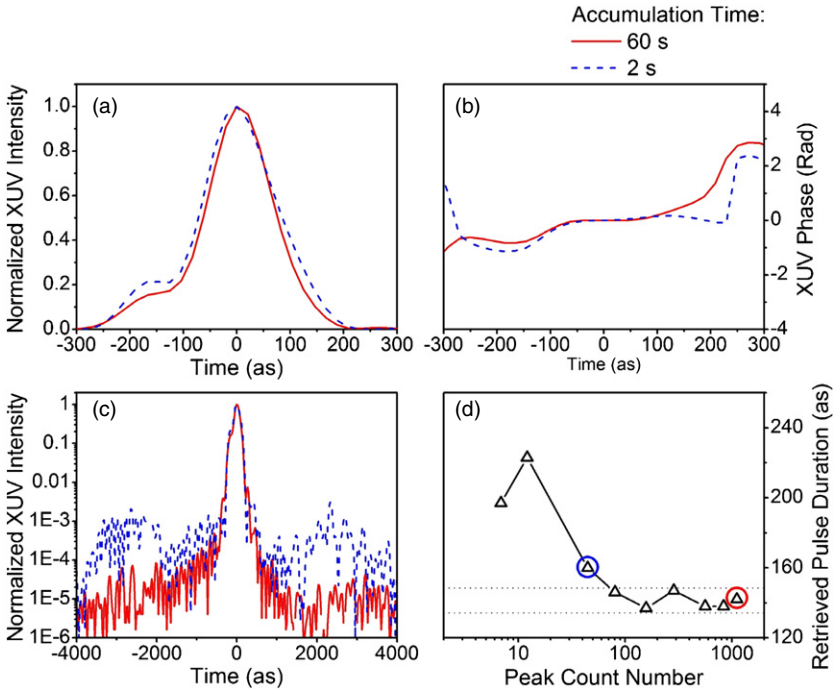


**Figure 7.** (a) Temporal profile of the retrieved attosecond pulse for 60 s (solid red line) and 2 s (dashed blue line) accumulation time. (b) Temporal phase of the retrieved pulse. (c) Log scale plot of the temporal profile. (d) Retrieved XUV pulse duration. The dotted lines indicate a window of ±5% centred at a duration of 141 as, which includes all of the retrieved pulse durations for accumulation times of 4 s and larger. The circles indicate the pulses shown in (a), (b) and (c). The peak counts measured here include the shot noise, and we thus expect that the roughly 80 counts at the peak of the two-dimensional spectrogram corresponding to 4 s accumulation time should relate quite closely to the 50 count simulations due to the statistical nature of the shot noise.

(This figure is in colour only in the electronic version)

### *4.1. The dependence of minimum streaking intensity on the XUV bandwidth*

When the PCGPA was applied on noisy data with a maximum count of 50 or more, it was found that even with a streaking intensity of $7.5 \times 10^{11}$ W cm$^{-2}$, nearly two orders of magnitude smaller than the value based on the Rayleigh criterion, PCGPA can correctly retrieve the XUV pulse with spectrum supporting a 90 as transform-limited pulse after 1000 iterations as shown in figures 6(a) and (b). As the maximum count increases, the retrieved pulse duration and chirp become closer to the actual values. In particular, for the XUV pulse with spectrum supporting a 180 as transform-limited pulse, the retrieved pulse duration converges in the same way for all the streaking intensities as the maximum count rate increases. Although this minimum streaking intensity is much less than the prediction from the classical streaking camera, our simulations show that it still depends on the bandwidth of the XUV pulse. As shown in figures 6(a) and (c), when the NIR streaking intensity is $5 \times 10^{11}$ W cm$^{-2}$, the pulse duration is never accurately reconstructed for pulses with spectrum supporting 90 as transform-limited pulses, whereas it is retrieved quite well for pulses with spectrum supporting 180 as transform-limited pulses as the peak count is increased. Therefore, for larger bandwidths, higher streaking intensities are required.

This conclusion is similar to the prediction from classical streaking camera and can be understood from the 2D pulse retrieval point of view. If the intensity of the NIR streaking field is zero, the CRAB trace is only a collection of XUV photoelectron spectra, and no phase information of the XUV pulse is embedded. As the intensity of the NIR streaking field is increased, the ratio between the streaked part and the unstreaked part in the CRAB trace also increases. If the CRAB trace is ideal and an infinite number of iterations of the PCGPA can be run, theoretically there always exists a unique solution to the CRAB trace even when the streaking intensity is low. However, the signal-to-noise ratio of CRAB trace is limited by the maximum count rate in the experiment, and the PCGPA cannot be run for an infinite number of iterations. Therefore, for experimental data the ratio between the streaked part and the unstreaked part in the CRAB trace must reach a threshold value for full characterization of the XUV pulses. In order to reach a similar ratio, spectra with larger bandwidth need to be streaked more, which corresponds to a higher minimum streaking intensity.

### *4.2. The dependence of minimum streaking intensity on XUV chirp*

Unlike optical FROG, in CRAB the NIR field acts only as a phase modulator in the time domain. When a chirped XUV pulse is streaked by the NIR field, the phase modulation from the NIR field either enhances or cancels the phase of the XUV pulse and generates a streaking trace with asymmetry in each NIR cycle, which contributes to the retrieval of the linear chirp parameters. Therefore, to discuss the minimum streaking intensity requirement in a more comprehensive way, the linear chirp of an XUV pulse with a spectrum supporting

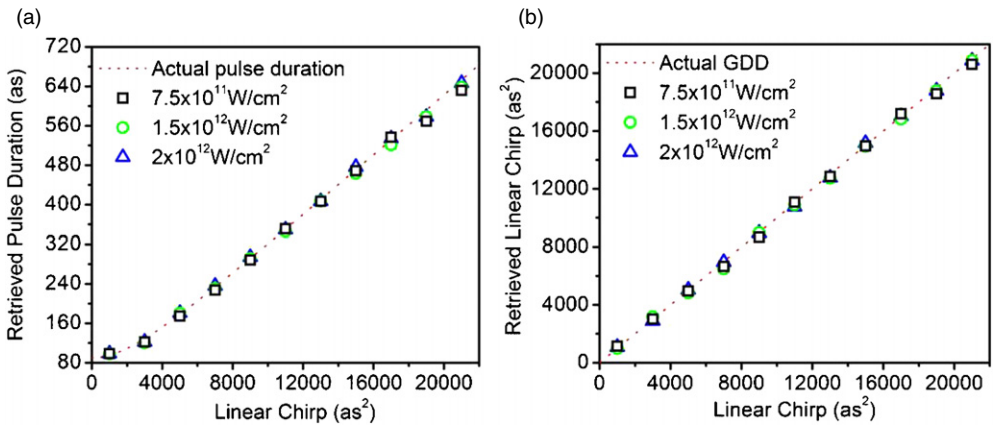


**Figure 8.** (a) Retrieved XUV pulse duration as a function of input linear chirp for different streaking intensities. (b) Retrieved linear chirp as a function of input linear chirp for different streaking intensities.
(This figure is in colour only in the electronic version)

a 90 as transform-limited pulse was scanned with the above streaking intensities. The peak count was set at 100 to satisfy the convergence discussion above. As shown in figures 8(a) and (b), even with the linear chirp of 20 000 as$^2$, for which the XUV pulse duration was broadened to one quarter of the NIR cycle, both the pulse duration and the linear chirp of the XUV pulse can be retrieved with high accuracy, which can be attributed to the advantage of 2D phase retrieval.

Thus the CRAB method requires much lower streaking intensity than the classical streaking camera method to measure the same isolated XUV pulse. This conclusion removes the NIR intensity constraint of measuring attosecond pulses, which is important for characterization of even shorter attosecond pulses.

## 5. Laser intensity variation

In the streaking experiments, the electrons are produced within a volume of the target gas determined by the XUV spot size and the length of the interaction region. Within this volume, the streaking laser intensity varies both transversely and longitudinally. Specifically, with the drilled mirrors or annular mirrors usually used to reflect and focus the streaking laser beam [9, 10, 15], a Bessel beam is produced at the focal point due to the truncation of the Gaussian beam. The spot size of the central Bessel spot is limited by the inner diameter of the drilled mirror or annular mirror and is smaller than the untruncated case. On the other hand, typical mirrors used to focus the XUV pulses to the target gas have surface accuracy distances many times larger than the XUV wavelength, which can lead to an XUV focal spot similar in size to the NIR focal spot. Photoelectrons born at different locations are thus streaked by different laser intensities, which causes smearing along the energy axis of the CRAB trace.

In order to study this effect, CRAB traces simulated using different NIR streaking intensities were averaged together and sent to the PCGPA for retrieval. We assumed the XUV and NIR focal spots to be Gaussian in shape, and weighted the average by the relative XUV photon number corresponding to each intensity. Figure 9 shows the retrieval results for XUV pulses with a spot size ratio of $w_{\mathrm{XUV}}/w_{\mathrm{IR}} = 0.5$, where $w_{\mathrm{XUV}}$ and $w_{\mathrm{IR}}$ are the $1/\mathrm{e}^2$ radii of the XUV and NIR focal spots. Because of the intensity averaging effect, the CRAB trace becomes blurred along the energy axis as is shown in figure 9(a). However, as is shown in figure 9(b), the PCPGA is able to retrieve a trace which matches the averaged trace very closely. In figure 9(c) the retrieved XUV pulse duration and phase exactly match the original values, and the retrieved gate phase from the averaged CRAB trace is nearly identical to the weighted average of the gate phases corresponding to each streaking intensity, as shown in figure 9(d).

For a more general test of the CRAB retrieval under intensity fluctuation, averaged CRAB traces with different $w_{\mathrm{XUV}}$ to $w_{\mathrm{IR}}$ spot size ratios were simulated. As shown in figures 10(a) and (b), when the XUV to NIR spot size ratio becomes larger than 0.5, the retrieved XUV pulse duration and phase start to deviate from the actual values. However, even when the XUV spot size is comparable to the NIR spot size at the focus, the XUV pulse duration and linear chirp can still be retrieved within an accuracy of 5%. This releases the constraint of constant streaking intensity and can easily be realized experimentally.

## 6. Collection angle of streaked electrons

Due to the low photon flux and small cross section of the XUV interaction with atoms, the streaked electrons are usually collected within a certain range of solid angle in order to maximize the count and reduce the statistical noise of the CRAB trace [10, 15, 26]. Since the gate phase is a function of the collection angle [13], the smearing effect should be taken into consideration when the CRAB trace is collected within a certain solid angle. In our simulation, we assume the asymmetric parameter to be $\beta = 1.4$ [27] to resemble the angular distribution of photoelectrons ionized from a neon gas target centred at 100 eV. The spherical integration and the angular distribution of the photoelectrons are multiplied together in the weighted average of the CRAB trace as shown in equation (12), where $\theta_0$ is the maximum collection angle, and $\bar{S}(W, \tau, \theta_0)$ is the averaged CRAB trace.

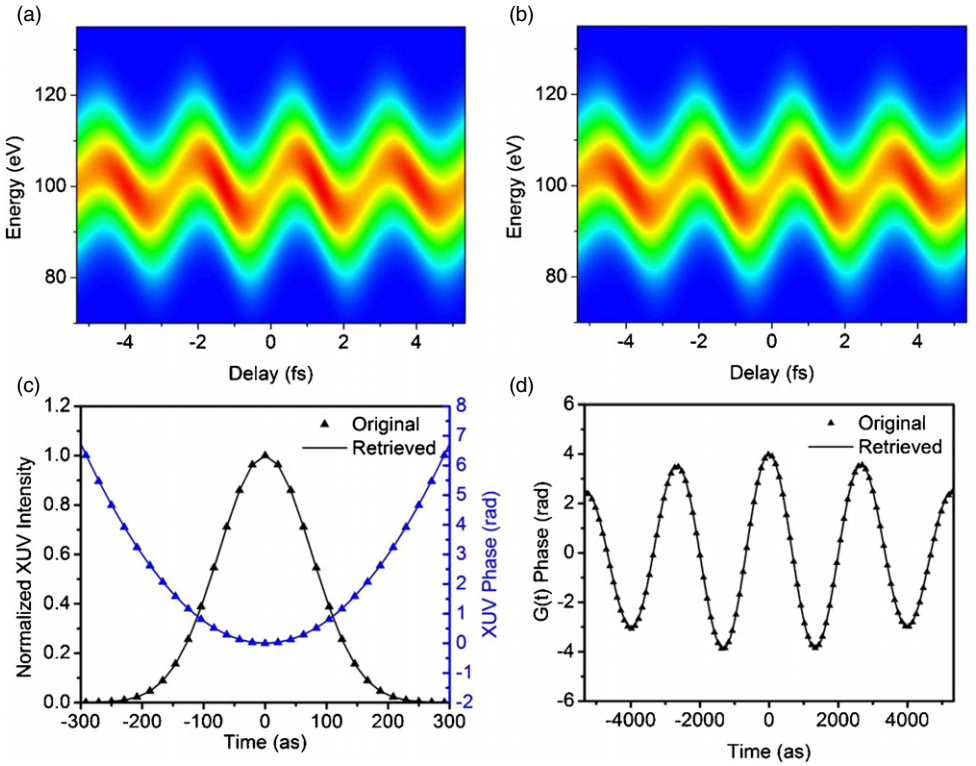


**Figure 9.** (a) Averaged CRAB trace when $w_{\mathrm{XUV}}/w_{\mathrm{IR}} = 0.5$. (b) Retrieved CRAB trace. (c) Original and retrieved XUV pulse and phase. (d) Original and retrieved gate phase.

(This figure is in colour only in the electronic version)

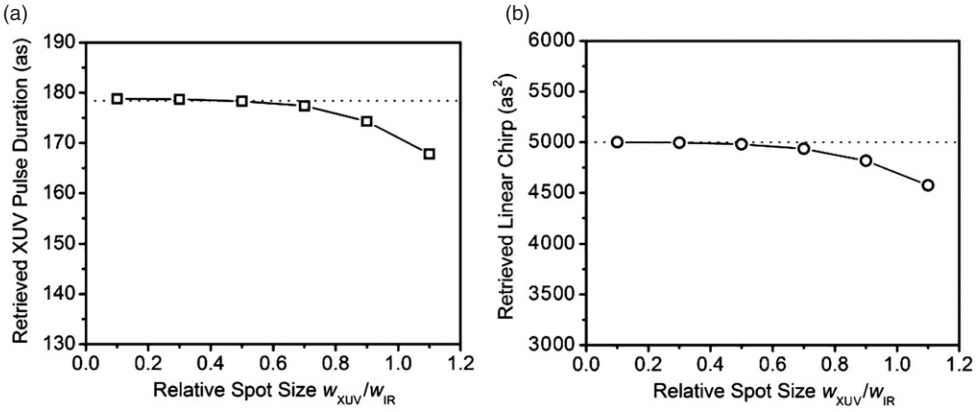


**Figure 10.** Retrieved (a) XUV pulse duration and (b) XUV linear chirp as a function of the spot size ratio $w_{\mathrm{XUV}}/w_{\mathrm{IR}}$. The red dashed lines indicate the actual values, whereas the black open shapes represent the retrieved values.

(This figure is in colour only in the electronic version)

$$\bar{S}(W,\tau,\theta_0) = \int_0^{2\pi}\int_0^{\theta_0} \hat{S}(W,\tau,\theta) \times \left[1+\frac{\beta}{2}(3\cos^2\theta - 1)\right]\sin\theta \mathrm{d}\theta\mathrm{d}\varphi, \quad (12)$$

In figure 11, when the maximum collection angle was set to 40°, the retrieved trace looks very similar to the averaged trace, and the XUV pulse duration and phase, as well as the NIR gate phase, are fully recovered.

Since in some experiments, such as those using magnetic bottle detectors or velocity map imaging, the total collection angle of the streaked photoelectrons can reach $2\pi$ or $4\pi$ solid angle, which corresponds to a maximum collection angle $\theta$ of 90° or 180°. However, due to the symmetry of the photoelectron emission, the CRAB trace resulting from a maximum collection angle of 180° should be identical to that from 90°. Therefore, we simulated CRAB traces for different maximum collection angles ranging from $\theta = 10°$ to 90°. As shown in figures 12(a) and (b), when the maximum collection angle is below 40°, the XUV pulse duration and chirp can be retrieved exactly. Even when the collection angle is further increased to 90°, for which the photoelectrons emitted orthogonally to the streaking laser polarization direction are also collected, the XUV pulse duration and linear chirp can still

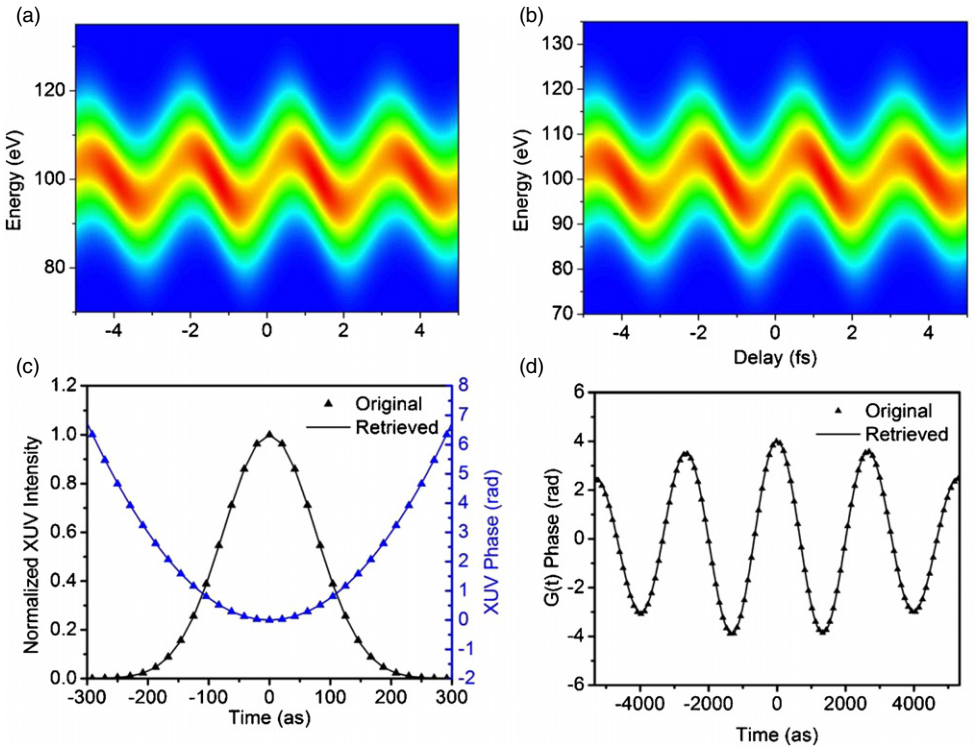


**Figure 11.** (a) Averaged CRAB trace when the maximum collection angle of photoelectrons is 40°. (b) Retrieved CRAB trace. (c) Original and retrieved XUV pulse and phase. (d) Original and retrieved gate phase.

(This figure is in colour only in the electronic version)

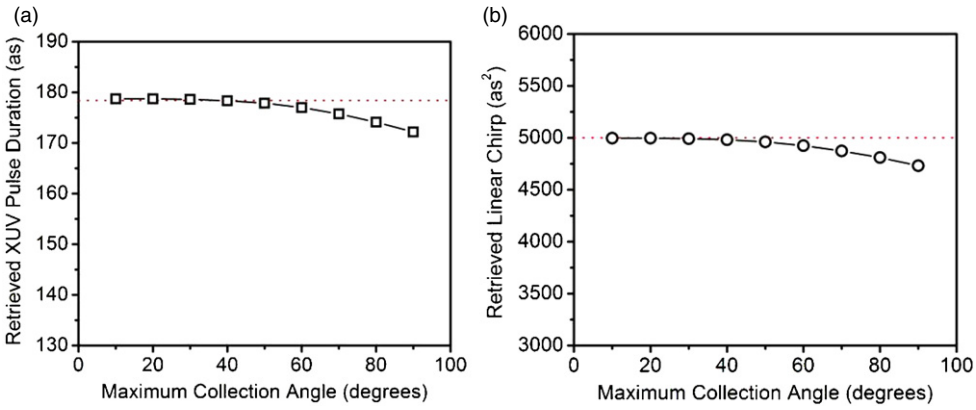


**Figure 12.** Retrieved (a) XUV pulse duration and (b) XUV linear chirp as a function of the maximum collection angle $\theta_0$. The red dashed lines indicate the actual values, whereas the black open shapes represent the retrieved values.

(This figure is in colour only in the electronic version)

be retrieved within an error of 5%. This property of the CRAB opens the door for detection schemes with large collection angles, such as magnetic bottle detectors and velocity map imaging [26, 28].

## 7. Time delay jitter

In the streaking experiment, the NIR streaking beam and XUV beam propagate through different optics. Due to mechanical vibration, the time delay between them fluctuates from one laser shot to the next [15], which broadens the CRAB trace along the delay axis. To study this effect on the final attosecond pulse reconstruction, a CRAB trace was generated by replacing the photoelectron spectrum at each delay step with the average of those from neighbouring delays. More specifically, the averaged CRAB trace is given by

$$\overline{S}(W, \tau, \Delta\tau_0) = \int_{-\Delta\tau_0/2}^{\Delta\tau_0/2} S(W, \tau + t)\, \mathrm{d}t, \qquad (13)$$

where $\Delta\tau_0$ is the delay jitter. In figure 13, when the delay jitter was ~200 as, comparable to the XUV pulse duration, the retrieved trace looks very similar to the averaged trace, and the XUV pulse duration and phase, as well as the NIR gate phase, are accurately retrieved. As shown in figures 14(a) and (b), when the delay jitter is ~100 as, the XUV pulse duration and chirp can be retrieved exactly. Even when the delay jitter goes to one quarter of the NIR laser cycle, the XUV pulse

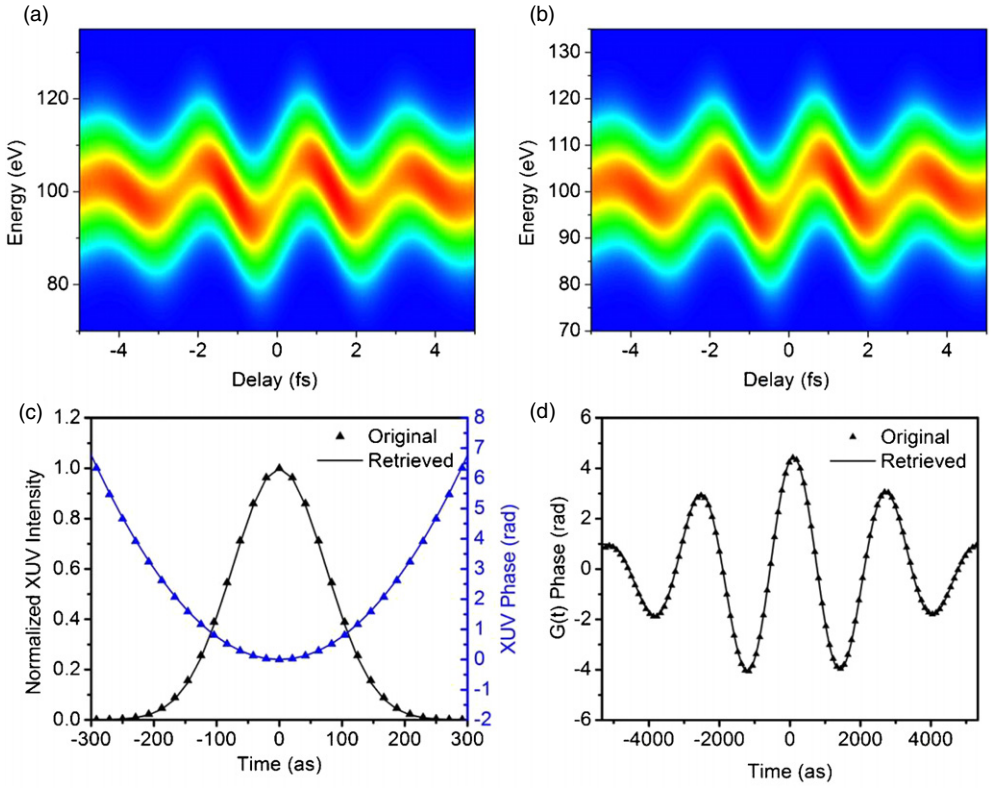


**Figure 13.** (a) Averaged CRAB trace when the time delay jitter is ∼200 as. (b) Retrieved CRAB trace. (c) Original and retrieved XUV pulse and phase. (d) Original and retrieved gate phase.
(This figure is in colour only in the electronic version)

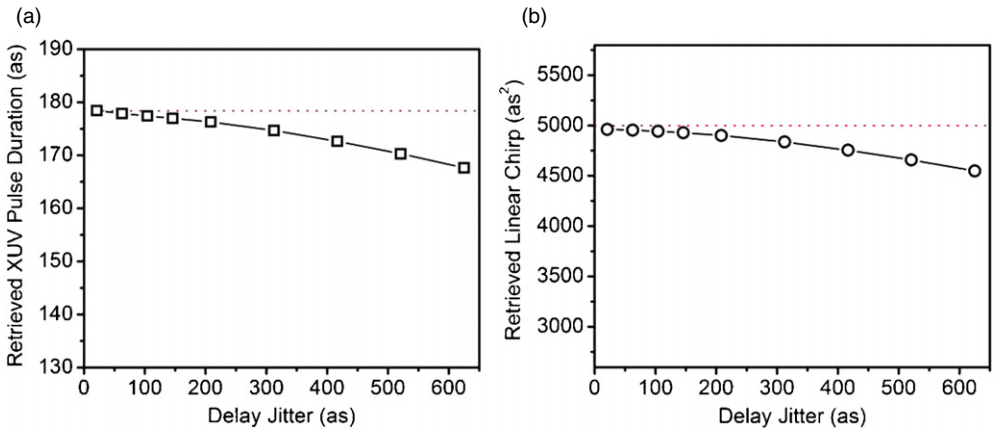


**Figure 14.** Retrieved (a) XUV pulse duration and (b) XUV linear chirp as a function of the time delay jitter. The red dashed lines indicate the actual values, whereas the black open shapes represent the retrieved values.
(This figure is in colour only in the electronic version)

duration can still be retrieved within an error of 6% and the linear chirp can be retrieved within an error of 10%. For streaking experiments with many-cycle streaking laser pulses for which the slowly varying envelope approximation holds, this type of timing jitter between the XUV and NIR pulses can also be interpreted as the fluctuation of the CE phase from one laser shot to the next. Thus, this property of the CRAB relaxes the need for tight CE phase locking and delay stability in streaking experiments.

## 8. Linearity discussion

The simulations of sections 5, 6 and 7 reveal the linear property of CRAB traces, i.e., the summation of two CRAB traces is approximately equal to a third physical CRAB trace. To shed some light on this property, we start from equations (1) and (2) and derive the analytical result of the spectrogram for a sufficiently short XUV pulse using the saddle point approximation [8].

$$S(W,\tau) \propto \frac{|d(\mathbf{p}+\mathbf{A}_{\mathrm{L}}(t_0+\tau))E_{\mathrm{X}}(t_0)|^2}{\mu} \times \exp\left\{-\left[\frac{(\mathbf{p}+\mathbf{A}_{\mathrm{L}}(t_0+\tau))^2}{2}-W_0\right]^2\frac{\tau_0^2}{\mu^2}\right\}, \quad (14)$$

where $\mu=\sqrt{(1+\eta\xi)^2+\eta^2}$ and $\eta=\mathbf{E}_{\mathrm{L}}(t_0+\tau)\mathbf{p}(t_0)\tau_0^2$. When $\mathbf{E}_{\mathrm{L}}$ and $\mathbf{A}_{\mathrm{L}}$ are small enough, we can Taylor expand equation (14) to a first-order approximation. The spectrogram can then be written as

$$\begin{aligned} S(W,\tau) \propto{}& |d(\mathbf{p}+\mathbf{A}_{\mathrm{L}}(t_0+\tau))E_{\mathrm{X}}(t_0)|^2 \\ &\times \exp\left[-\left(\frac{p^2}{2}-W_0\right)^2\tau_0^2\right] \\ &\times\left[1-2\mathbf{A}_{\mathrm{L}}(t_0+\tau)\mathbf{p}\left(\frac{p^2}{2}-W_0\right)\tau_0^2+2\mathbf{E}_{\mathrm{L}}(t_0+\tau)\right. \\ &\left.\times\,\mathbf{p}\left(\frac{p^2}{2}-W_0\right)^2\xi\tau_0^4-\mathbf{E}_{\mathrm{L}}(t_0+\tau)\mathbf{p}\tau_0^2\xi\right]. \end{aligned} \quad (15)$$

From equation (15), the streaked spectrogram can be decomposed into an unstreaked spectrogram multiplied by terms that have a linear relationship with $\mathbf{A}_{\mathrm{L}}$ and $\mathbf{E}_{\mathrm{L}}$. The averaged values $\bar{\mathbf{A}}_{\mathrm{L}}$ and $\bar{\mathbf{E}}_{\mathrm{L}}$ for any accumulated spectrogram from different $\mathbf{A}_{\mathrm{i}}$ and $\mathbf{E}_{\mathrm{i}}$ can be expressed as

$$\bar{\mathbf{A}}_{\mathbf{L}}=\frac{\sum\rho_i\mathbf{A}_i}{\sum\rho_i}, \quad (16)$$

$$\bar{\mathbf{E}}_{\mathbf{L}}=\frac{\sum\rho_i\mathbf{E}_i}{\sum\rho_i}, \quad (17)$$

where $\rho_i$ is the weight of $\mathbf{A}_{\mathrm{i}}$ and $\mathbf{E}_{\mathrm{i}}$. This shows that a linear combination of different $\mathbf{A}_{\mathrm{i}}$ and $\mathbf{E}_{\mathrm{i}}$ can still yield a spectrogram as if it is streaked by an average value of $\bar{\mathbf{A}}_{\mathrm{L}}$ and $\bar{\mathbf{E}}_{\mathrm{L}}$ with the same XUV pulse. The error of equation (15) is introduced by dropping all higher order terms, and is dominated by the second-order term $(\mathbf{A}_{\mathrm{L}}\mathbf{p}\tau_0)^2$. This indicates that the linear property of the spectrogram is more prominent when the transform-limited XUV pulse duration is short and the streaking field is weak.

## 9. Conclusions

We have shown that shot noise has little effect on the retrieval of single attosecond pulses with PCGPA for traces with at least 50 photoelectron counts at the peak of the photoelectron spectrum, provided the streaking laser intensity is greater than the minimum streaking intensity. In fact, the algorithm has been shown to always converge to a result closer to the noise-free-simulated trace than to that with noise added, and retrieves pulses with duration and linear chirp within 5% of the simulated pulses for maximum pixel counts of at least 50. Such a result is significant, as it suggests a lower limit to the number of counts necessary for accurate attosecond pulse retrieval. Due to the difficulty in maintaining identical CE phase stabilized laser pulses over a long period of time, this makes measurement of single attosecond pulses more accessible to laboratories without state-of-the-art laser systems. Furthermore, we found that the minimum streaking field intensity needed for accurate reconstruction from a noisy CRAB trace can be nearly two orders of magnitude lower than that estimated from the classical streaking model. Such a low streaking field intensity is desirable to suppress the ATI background. However, for larger XUV bandwidths, higher streaking intensities are required, which agrees with the classical prediction qualitatively. Because of the linear property of the CRAB trace, the reconstruction is robust against time jitter between the XUV and streaking fields, intensity variation of the streaking field and collection angle of the streaked electrons. These conclusions are important for the characterization of even shorter XUV attosecond pulses because they significantly reduce the constraints on the experiments.

## Acknowledgments

The authors would like to thank Dr Brian Washburn for helpful discussions. This material is supported by the U.S. Army Research Office under grant number W911NF-07-1-0475, and by the Chemical Sciences, Geosciences and Biosciences Division, Office of Basic Energy Sciences, Office of Science, U.S. Department of Energy.

## References

[1] Drescher M *et al* 2002 *Nature* **419** 803
[2] Keinberger *et al* 2004 *Nature* **427** 817
[3] Goulelmakis *et al* 2007 *Science* **317** 769
[4] Uiberacker M *et al* 2007 *Nature* **446** 627
[5] Kling M F *et al* 2008 *Conference on Lasers and Electro-Optics (CLEO), paper JFH1*
[6] Cavalieri A L *et al* 2007 *Nature* **449** 1029
[7] Hentschel M *et al* 2001 *Nature* **414** 509
[8] Itatani J, Quéré F, Ivanov M Y, Krausz F and Corkum P B 2002 *Phys. Rev. Lett.* **88** 173903
[9] Sansone G *et al* 2006 *Science* **314** 443
[10] Goulielmakis E *et al* 2008 *Science* **320** 1614
[11] Gagnon J, Goulielmakis E and Yakovlev V 2008 *Appl. Phys.* B **92** 25
[12] Kane D J 2008 *J. Opt. Soc. Am.* B **25** A120
[13] Mairesse Y and Quéré F 2005 *Phys. Rev* A **71** 011401
[14] Kitzler M, Milosevic N, Scrinzi A, Krausz F and Brabec T 2002 *Phys. Rev. Lett.* **88** 173904
[15] Chang Z 2008 *Proc. Int. Symp. in Utrafast Laser Science* vol 7, Kyoto, 24–28 November
[16] Mashiko H, Gilbertson S, Li C, Moon E and Chang Z 2008 *Phys Rev.* A **77** 063423
[17] Lee P and Weissler G L 1952 *J. Opt. Soc. Am.* **42** 214
[18] Tzallas P, Skantzakis E, Kalpouzos C, Benis E P, Tsakiris G D and Charalambidis D 2007 *Nat. Phys.* **3** 846
[19] Mashiko H *et al* 2008 *Phys. Rev. Lett.* **100** 103906
[20] Wang H *et al* 2007 *Appl. Phys* B **89** 275
[21] Li C, Moon E and Chang Z 2006 *Opt. Lett.* **31** 3113
[22] Fittinghoff D N, DeLong K W, Trebino R and Ladera C L 1995 *J. Opt. Soc. Am.* B **12** 1955
[23] Paulus G G, Crasbon F, Dreischuh A and Walther H 2000 *Phys. Rev. Lett.* **84** 3791
[24] Drescher M *et al* 2001 *Science* **291** 1923
[25] Kane D J and Trebino R 1993 *IEEE J. Quantum Electron.* **29** 571
[26] Mauritsson J, Johnsson P, Gustafsson E, L'Huillier A, Schafer K J and Gaarde M B 2006 *Phys. Rev. Lett.* **97** 013001
[27] Kennedy D J and Manson S T 1972 *Phys. Rev.* A **5** 227
[28] Mauritsson J *et al* 2008 *Phys. Rev. Lett.* **100** 073003